Essentials in Ophthalmology

Medical Retina

Focus on Retinal Imaging

Bearbeitet von
Frank G Holz, Richard F. Spaide

1. Auflage 2010. Buch. XVI, 227 S. Hardcover
ISBN 978 3 540 85539 2
Format (B x L): 19,3 x 26 cm
Gewicht: 695 g

Chapter 2

Simultaneous SD-OCT and Confocal SLO-Imaging

2

Peter Charbel Issa, Monika Fleckenstein, Hans-Martin Helb, Hendrik P. N. Scholl, Steffen Schmitz-Valckenberg, and Frank G. Holz

Core Messages

- Pathological findings visible on high-resolution optical coherence tomography (OCT) can be correlated with findings on confocal scanning laser ophthalmoscopy (cSLO) imaging, including fluorescein- and ICG- angiography, fundus autofluorescence (FAF) – or reflectance images, in exact topographic correspondance. Simultaneous acquisition is time-efficient and facilitates correlation of findings in the different imaging modalities.
- Eye tracking allows for stabilizing SD-OCT scans on areas of interest and averaging of multiple scans to improve image contrast.
- Exact alignement of serial examinations at the same retinal location enables to accurately track the disease course or treatment effects.

2.1 Background

Both optical coherence tomography (OCT) and confocal scanning laser ophthalmoscopy (cSLO) are increasingly used in a routine clinical setting for diagnostic purposes and assessment of treatment effects. They have also become valuable research tools due to their ability to assess retinal morphology in vivo [1, 2].

Recently, spectral domain (SD)-OCT with its advantage of high-resolution image acquisition has become commercially available. In previous (time-domain) OCT generations, reference mirrors move mechanically, which limits imaging speed. In SD-OCT, the reference mirror is stationary, and the OCT signal is acquired either by using a spectrometer as detector or by varying the narrowband wavelength of the light source in time. The resulting high-speed scan acquisition minimizes motion artifacts and enables the acquisition of three-dimensional volume OCT scans consisting of a multitude of individual scans without major interpolation [3].

In retinal imaging, confocality allows one to record alterations of a given plane with improved contrast and detail compared with conventional fundus photography. Commercially available cSLOs allow recording of various image modalities such as fluorescein and indocyanine green (ICG) angiography, fundus autofluorescence (FAF), or blue- and near-infrared reflectance images [4]. Especially, the noninvasive methods such as FAF imaging have recently gained increasing attention since they allow assessing and following alterations of the pigment epithelium with great detail [2].

2.2 Principle of the Combined Imaging Technology

A new device for retinal imaging, the Spectralis HRA+OCT (Heidelberg Engineering, Heidelberg, Germany) combines the two techniques in one instrument with various subsequent advantages including exact correlation of tomographic and topographic findings [3]. It allows to simultaneously record SD-OCT scans with fluorescein and ICG angiography, digital infrared and blue reflectance ("redfree"), or FAF images. The optical and technical principles of the cSLO unit are identical to a recently introduced instrument for clinical use, HRA2 (Heidelberg Engineering) [4]. In brief, an optically pumped solid-state laser source is used to generate the blue light excitation wavelength of 488 nm for fluorescein angiography, blue reflectance, and FAF images. Diode laser sources of 790 and 820 nm wavelength are used for ICG angiography and infrared reflectance recordings, respectively. The light safety calculations consider the specific optical setup and computer control of the device, and maximum retinal irradiance lies below the limits established by the American National Standards

Institute (ANSI) and other international standards (The Laser Institute of America 1993). Emission is recorded between 500 and 700 nm with a detection efficiency of 85% for fluorescein angiography and FAF images, and above 810 nm with a detection efficiency of 66% for ICG recordings. In the blue reflectance and infrared reflectance mode, the barrier filter is removed and the reflected light is directly recorded.

For automated alignment of the SD-OCT with the cSLO images, the software uses a sophisticated algorithm to detect eye movements between different images. A set of hundreds of landmarks is extracted automatically for every image. A combinatorial algorithm is used to match the landmarks between the different images. Six transformation parameters (two-dimensional affine transformation) are computed from the positions of the matching landmarks using a least square algorithm resulting in subpixel accuracy. The automated alignment is used for both real-time compensation of eye movements and averaging of multiple images. Assuming a Gaussian noise distribution in the image signal over time, the signal-to-noise ratio is increased by a factor of square-root of the number of images averaged, e.g., averaging over nine images will increase the signal-to-noise ratio in the generated mean image by a factor of 3.

The new operation software (ART – "Automatic Real Time" – Module, Heidelberg Engineering) is able to track eye movements in real time based on the cSLO images. Depending on the eye movements, the OCT B-scan is repositioned and thus stabilized and frozen at the retinal location selected. B-scans recorded during movement of the eye are discarded. The software then computes and compensates for movements between the B-scan images caused by the varying blood pressure and position changes of the eye relative to the camera, and finally averages the live B-scans, and thus, greatly enhances the image quality leading to remarkable B-scan detail and contrast because of a marked reduction in speckle and other noise.

The optics of the instrument allow for compensation of between −24 and + 30 diopters of ametropia in steps of 0.25 diopters. An internal fixation target from an array of 3 × 3 blue lights can be chosen individually by the examiner. Alternatively, an external target for fixation with the fellow eye may be used. Most operation settings are controlled via an interactive touch panel.

With regard to the OCT, 40,000 A-scans are acquired per second with a 7 µm axial optical resolution and a 14 µm lateral optical resolution. OCT scans can be recoded simultaneously with fluorescein angiography, ICG angiography, FAF, infrared and blue reflectance images. For the A-scans, the scan depth is 1.8 mm/512 pixels providing a digital axial resolution of 3.5 µm/pixel.

B-scans cover a transversal range of 15, 20, or 30° field of view. In the high-speed mode, scan widths are 384, 512, and 768 A-scans per B-scan with a lateral digital resolution of 11 µm/pixel and a scan rate of 89, 69, and 48 B-scans/sec. The high-resolution modes encompass a scan width of 768, 1,024, and 1,536 A-scans per B-scan with a lateral digital resolution of 5 µm/pixel at a scan rate of 48, 37, and 25 B-scans/sec.

Sequences of B-scans can be acquired to image a full volume. A large variety of patterns may be used, differing, e.g., in scan density, resolution, and orientation. The number of B-scans per volume can be adjusted from 12 B-scans per 10° to 96 B-scans per 10°. This results in a distance between consecutive parallel B-scans of approximately 30–240 µm.

All OCT images are automatically enlarged in the axial direction to improve visualization of intraretinal layers. Evaluation of OCT B-scans is done using a gray-scale visualization with a white background, which allowed for better recognition of details, especially in comparison with color-scale visualization as commonly used in time-domain OCT imaging [5].

Summary for the Clinician

- New combined imaging instruments allow studying regions of interest located on cSLO images (reflectance images, autofluorescence imaging, fluorescein angiography, or ICG angiography) with quasi in vivo histology of high-resolution SD-OCT sections. Moreover, automatic re-alignment allows for an accurate monitoring of retinal pathologies.

2.3 Clinical Application

OCT scans are presented underneath a topographic image in which an arrow marks the location and direction of the scan. Therefore, all structures on the two imaging modalities may be matched by drawing an imaginary vertical line from a point of interest in the topographic image to the OCT scan, and vice versa.

Figure 2.1 shows normal findings in the absence of retinal disease. The line in the infrared reflectance cSLO-image indicates where the OCT cross-section was obtained. There is still debate on the correlation of the various retinal layers with histological sections. However, the assignment as shown in the figure is now widely accepted.

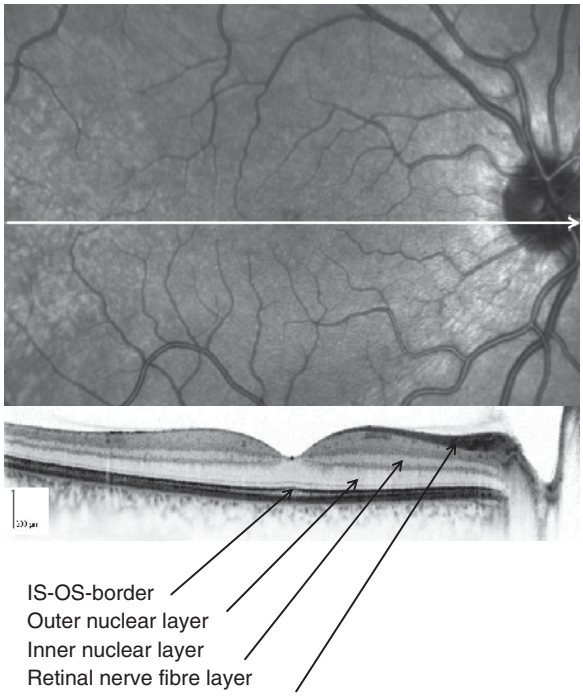

Fig. 2.1 The *white arrow* in the near-infrared confocal reflectance image shows the location where the correspondent OCT scan below is recorded. For reference, some retinal layers are assigned

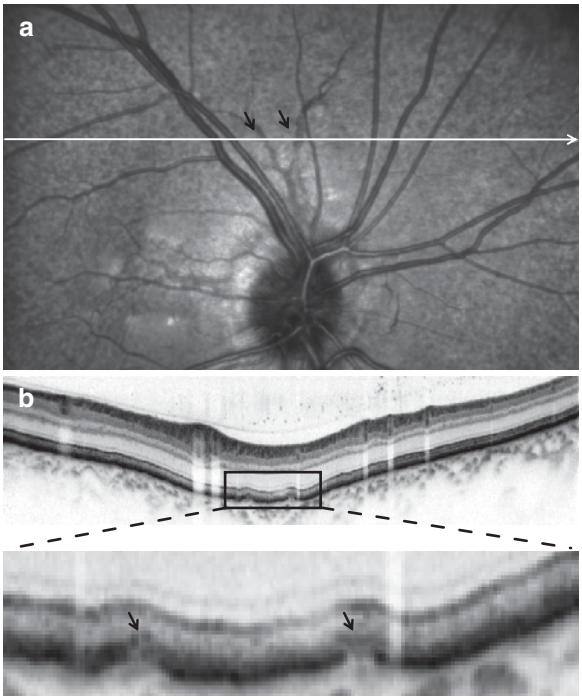

Fig. 2.2 Near-infrared reflectance image (**a**) and simultaneous OCT imaging (**b**) in a patient with peau d'orange and angioid streaks due to pseudoxanthoma elasticum. The black *arrows* point out the location of the angioid streaks

Figure 2.2 demonstrates findings on near-infrared fundus reflectance imaging in a patient with pseudoxanthoma elasticum (PXE). Near-infrared light is only marginally absorbed by the melanin in the retinal pigment epithelium (RPE). Therefore, the superior visibility of peau d'orange in this imaging mode may be explained by the location of the respective pathology below the RPE, i.e., within Bruch's membrane [6]. The simultaneously recorded SD-OCT scan crosses two angioid streaks (black arrows) and reveals a rupture in the thickened Bruch's membrane as pathological substrate. The overlying neurosensory retina appears intact.

Figure 2.3 shows the fundus of a 35-year-old myopic patient with a recent onset multiple evanescent white dot syndrome (MEWDS) in the right eye. In late-phase ICG angiography (25 min), the white dots may be better visualized than on fundus photography, fluorescein angiography, or FAF. The SD-OCT through the lesions revealed that structural alterations of the photoreceptor layer occur within the areas of white dots. This defect within the border of the inner and outer photoreceptor segments may be more widespread and persistent than expected from angiographic imaging [7, 8].

Figure 2.4 illustrates the findings on FAF and SD-OCT in a patient with severe rod-cone dystrophy due to a mutation in the MERTK gene. The MERTK protein plays a key role in the photoreceptor outer segment ingestion by the RPE during their physiological renewal [9]. In animal models with *MERTK* mutations, debris accumulates in the subretinal space due to the inability of the pigment epithelium to clear shed photoreceptor outer segments [10]. By means of SD-OCT, it was possible to detect analogous subneurosensory debris in the affected patients in vivo [11]. Moreover, simultaneous FAF imaging revealed that marked atrophy within the photoreceptor layer is associated with loss of FAF due to atrophy of the pigment epithelium.

Figure 2.5 presents serial simultaneous SD-OCT and near-infrared reflectance imaging (follow-up period 10 months) in geographic atrophy due to age-related macular degeneration (AMD). SD-OCT has recently allowed further study into the morphological changes in geographic atrophy in a quasi-histological manner [12, 13]. The exact re-location of the OCT scan in follow-up exams now enables the study of areas of geographic atrophy and their changes over time longitudinally. Within atrophic areas, the outer retina including the RPE and the outer

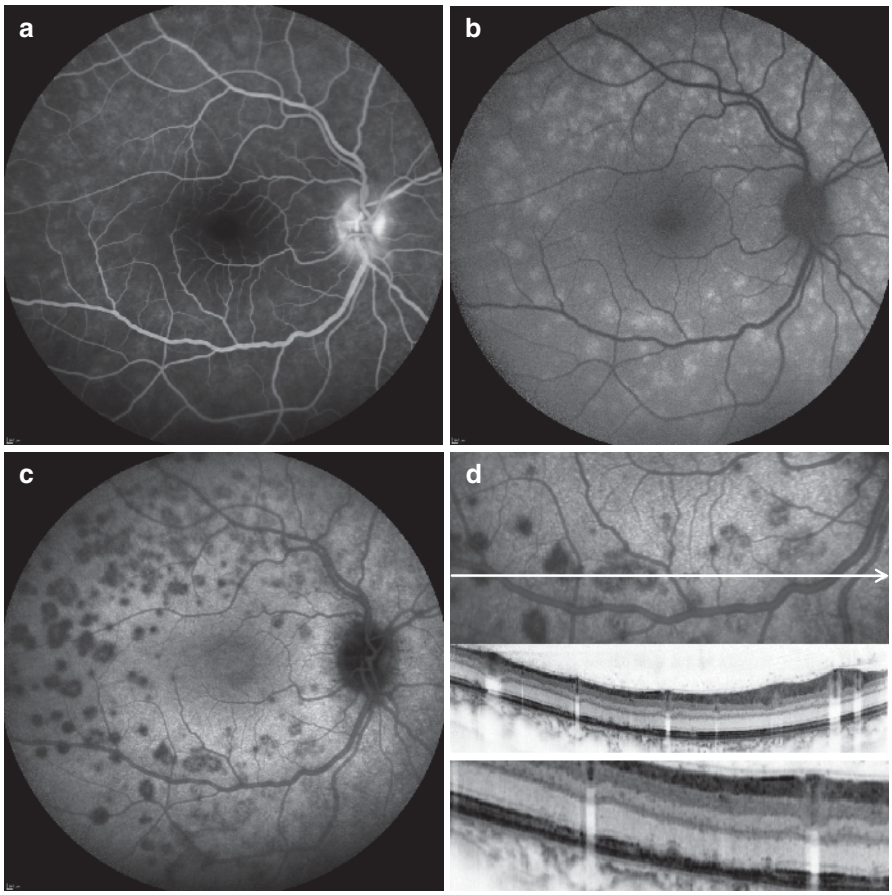

Fig. 2.3 Fluorescein angiography (**a**), FAF (**b**), late-phase (25 min) ICG angiography (**c**), and simultaneous OCT imaging (**d**) in an acute stage of MEWDS. The lesions show a superior visibility on late-phase ICG angiography. The simultaneous OCT reveals that the pathology appears to affect the outer neurosensory retina

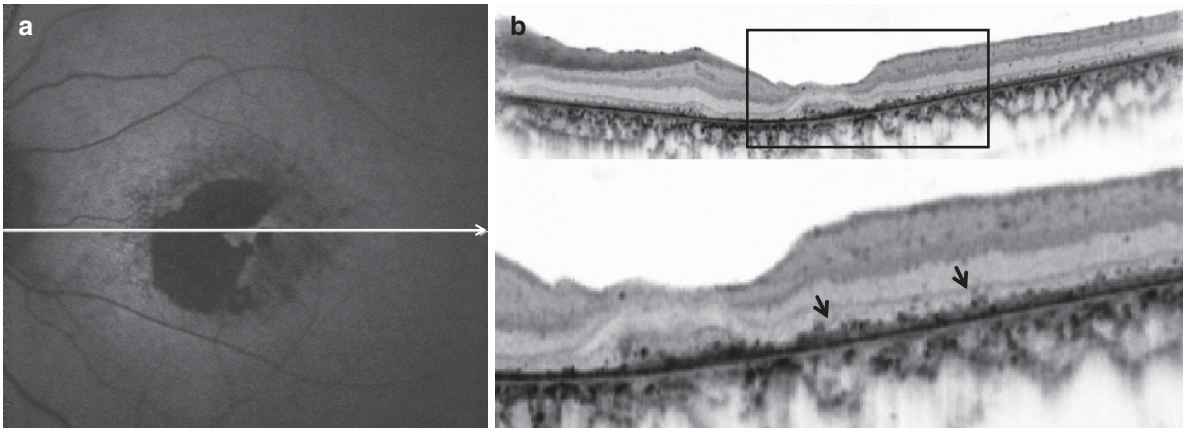

Fig. 2.4 Fundus autofluorescence (FAF) in a patient with rod-cone dystrophy due to a mutation in the MERTK gene (**a**). There was an overall reduced FAF and an area of pigment epithelial atrophy. Simultaneous SD-OCT imaging (**b**) revealed debris above the retinal pigment epithelium (black *arrows*)

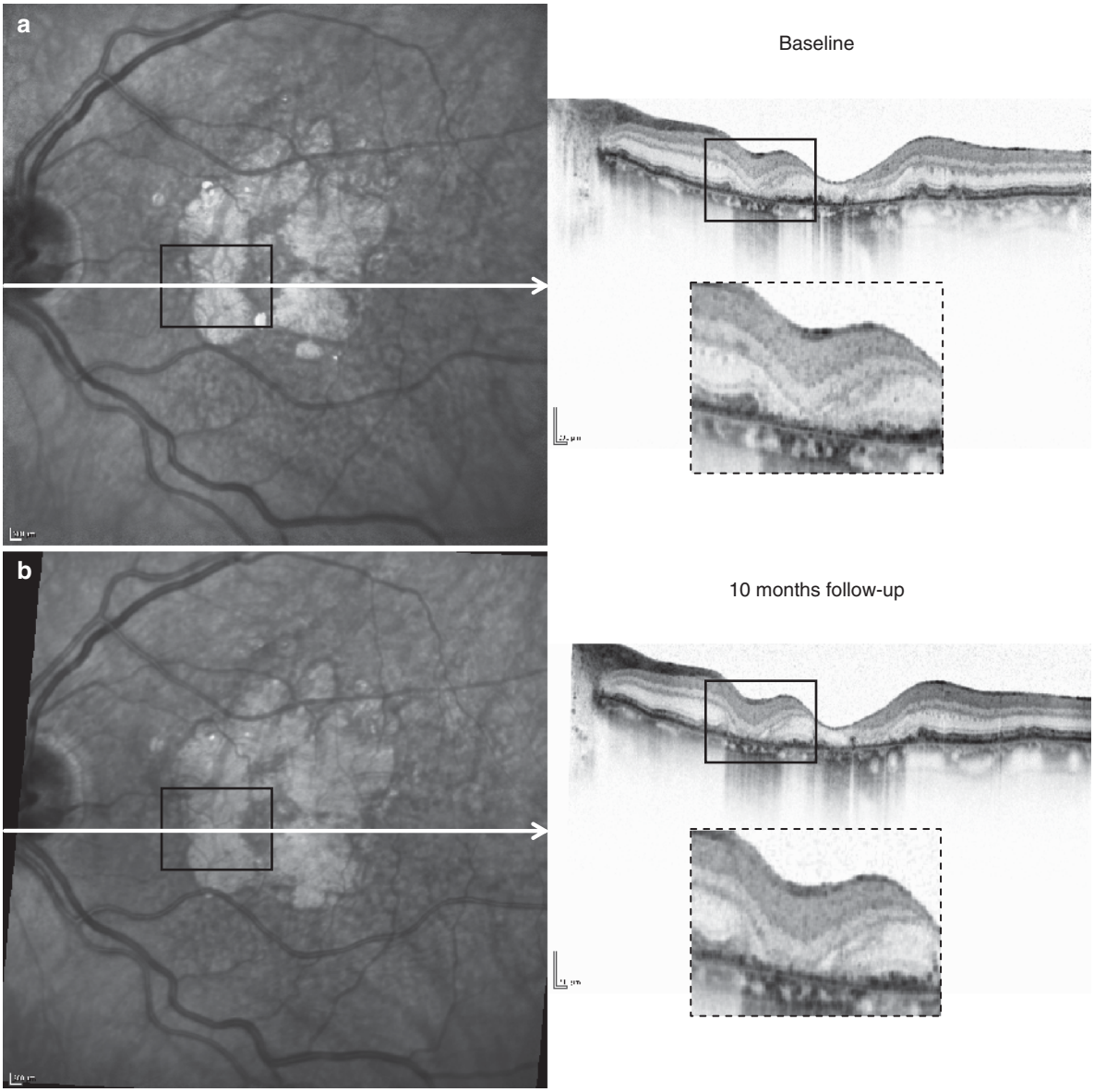

Fig. 2.5 Changes over time within a patch of geographic atrophy due to age-related macular degeneration (AMD) in a 77-year-old patient. (**a**) Infrared reflectance image and the corresponding OCT scan at baseline and (**b**) at follow-up 10 months later. Enlargement of the atrophic area occurred in conjunction with progressive atrophy within the outer retinal layers. Dashed boxes are magnifications of the boxes highlighted in the OCT scan above

nuclear layer appear atrophic on the OCT scan, resulting in close approximation of the inner retinal layers to Bruch's membrane. Compared with baseline (A), the area of outer retinal atrophy was larger at 10 months follow-up (B). The box highlights an area with enlargement of a small atrophic lesion over time.

Figure 2.6 shows a pigment epithelial detachment (PED) in a patient with neovascular AMD. It is noteworthy that the PED goes beyond the area with obvious hyperfluorescence on late-phase angiography. This is due to the masking of the angiographic leakage by macular pigment, resulting in the appearance that the foveal center would be spared.

Figure 2.7 shows the right eye of a patient with macular telangiectasia (MacTel) type 2. On ophthalmoscopy, there is often the appearance of a lamellar macular hole, which appears dark on confocal blue reflectance imaging (A). Simultaneous SD-OCT imaging reveals that the correlates on OCT imaging are foveal hyporeflective spaces within the neurosensory retina (C). In MacTel type 2, there is a

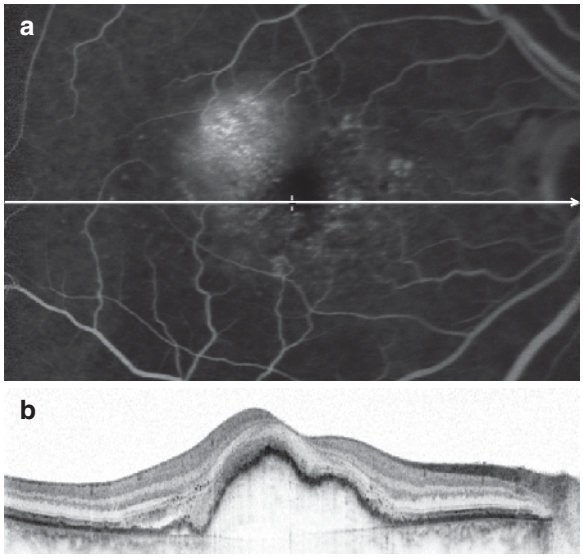

Fig. 2.6 Simultaneous fluorescein angiography and OCT examination in a patient with a pigment epithelial detachment due to AMD. Note the discrepancy between the apparent sparing of the foveal center on angiography (**a**) and the true expansion of the lesion involving the foveal center on OCT imaging (**b**)

characteristic late-phase leakage on fluorescein angiography within the parafoveolar area (B). The hyporeflective retinal spaces show no pooling on fluorescein angiography which is in contrast with other cystoid spaces as in exudative macular edema. These spaces have also been shown to exhibit an internal reflectivity different from exudative cystoid spaces [14]. It was concluded that hyporeflective spaces in MacTel type 2 are rather due to atrophic neurosensory alterations than having an exudative origin.

Figure 2.8 presents findings in two patients with isolated foveal hypoplasia [15]. Patient 1 was 54-year-old and presented with a visual acuity of 20/32. Patient 2 was a 9-year-old boy with bilateral unexplained low visual acuity. Visual acuity was 20/63 in the right eye and 20/50 in the left eye and a slow rotating nystagmus was present. In both patients, there was no foveolar and macular reflex. Patient 1 showed an overall light pigmentation of the peripheral fundus and a conspicuous course of the retinal vessels at the posterior pole. FAF imaging revealed a lack of macular pigment and three-dimensional OCT volume scans could not detect a foveal pit. All neurosensory retinal layers were continuous throughout the foveal center.

2.4 Conclusions

Recent improvement in OCT imaging, including increased resolution and image-contrast, a noninvasive visualization of the microstructural retinal morphology

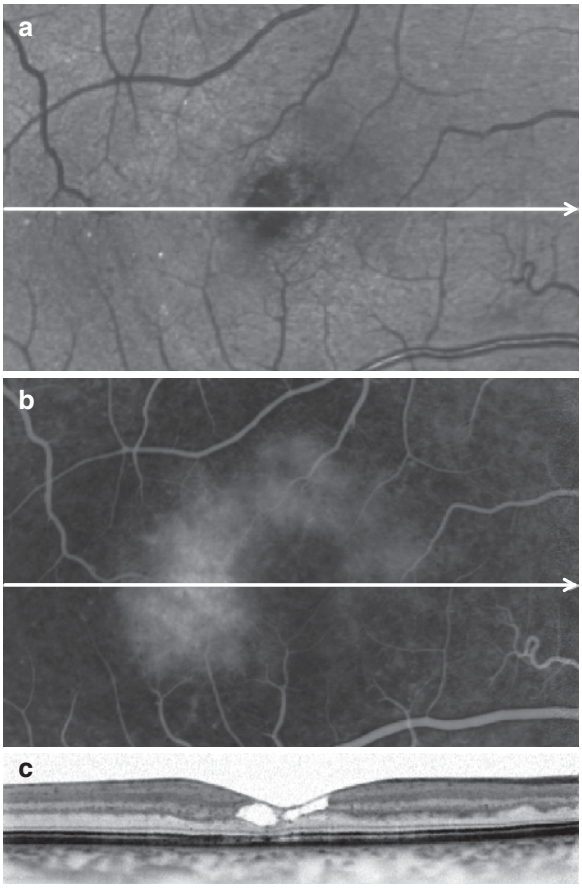

Fig. 2.7 Simultaneous confocal blue reflectance imaging (**a**) or late phase fluorescein angiography (**b**) with SD-OCT (**c**) in a patient with macular telangiectasia type 2. The small dark foveal area in (**a**) appears as a lamellar macular hole on ophthalmoscopy. The correlates on the SD-OCT scan are characteristic hyporeflective spaces within the neurosensory retina. There is no pooling of fluorescein in those cystoid spaces

in vivo. The combination of these new OCT technologies and topographic cSLO imaging within one instrument as described here allows studying the cross-sectional structure of regions of interest on fluorescein and ICG angiography, blue or infrared reflectance, and FAF imaging. This possibility will further improve our understanding of the pathogenesis of macular pathologies and may prove to be useful for diagnosis and patient management.

There is a broad range of potential research and clinical applications for this new instrument. For example, monitoring the natural history or treatment effects in patients with AMD will be facilitated. When the patient returns for follow-up examination, it is now possible to evaluate changes on OCT imaging at precisely the same retinal location as in the previous examination due to the

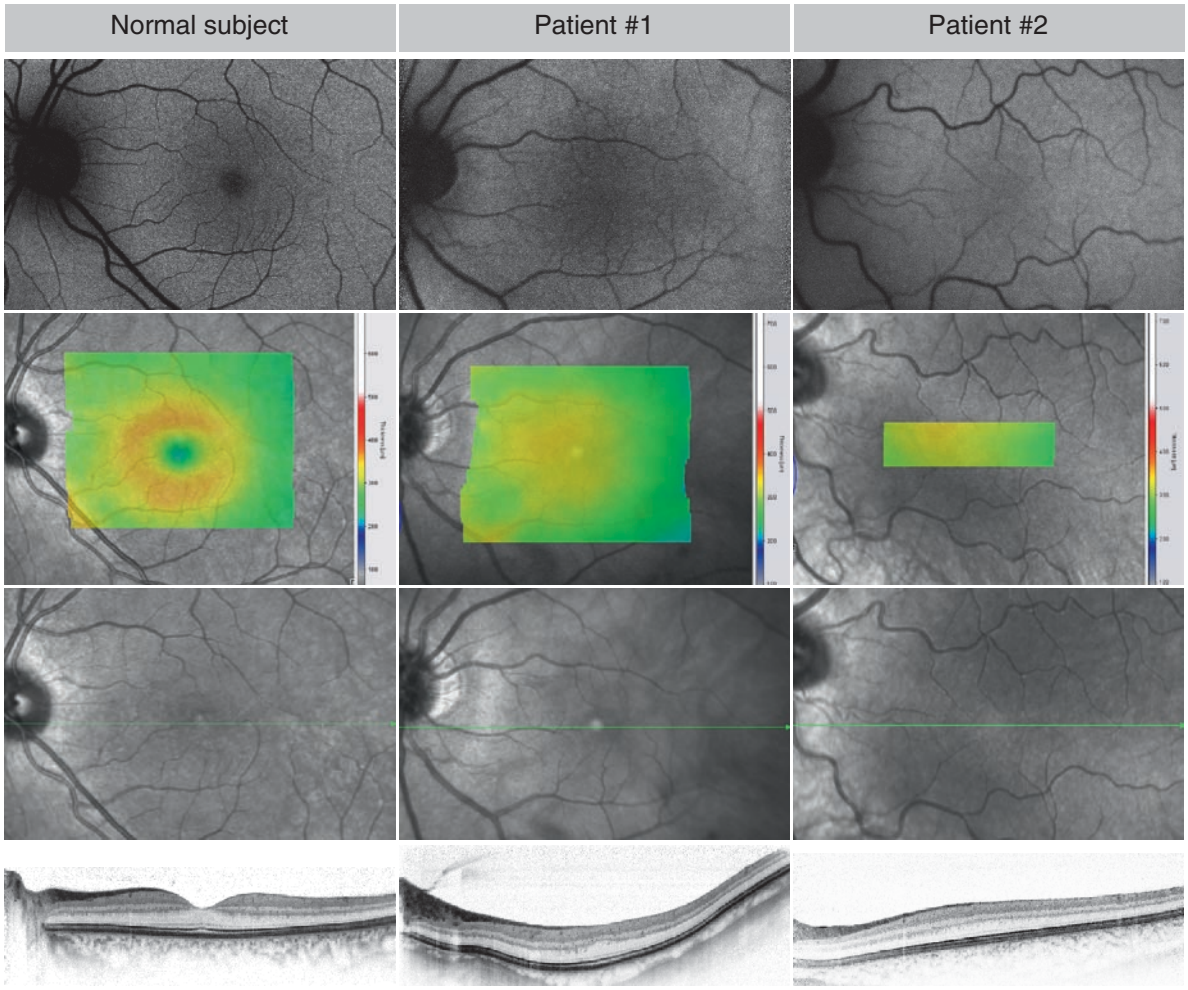

Fig. 2.8 (From Ref. [15] with permission): Left eye of a normal subject (for comparison) and two patients with foveal hypoplasia. Both patients show reduced (Patient 1) or almost absent (Patient 2) macular pigment on FAF imaging (*first row*). The color-coded retinal thickness maps reveal absence of the foveal pit in both patients. The infrared confocal reflectance image (*third row*) shows the location of the OCT-scan below (*green line*). In the patients, all retinal layers continue through the presumed foveal area on OCT scans and no foveal contour is present.

automated re-alignment of the OCT scans. This allows for more reliability to judge on whether or not retinal fluid accumulation has stayed the same, increased, or decreased, even if changes are only small. This information may be crucial regarding advice for re-treatment. Moreover, the combined assessment is less time-consuming and therefore more cost-effective than performing the two imaging modalities sequentially.

Besides these advantages for follow-up examinations, the automated eye-tracker allows for the averaging of multiple OCT scans at exactly the same location, resulting in a superior signal-to-noise ratio (i.e., improved image contrast) compared with nonaveraged images. It furthermore ensures that subsequent OCT scans during the acquisition of volume scans are placed at the foreseen location, independent of eye movements.

FAF imaging combined with spatially correlated OCT offers new research applications. The FAF signal mainly derives from lipofuscin granules in the RPE [16]. Excessive lipofuscin accumulation is a common pathogenetic pathway in various retinal diseases including monogenic disorders such as Stargardt's or Best's disease and complex diseases such as AMD [2, 17]. Recently, FAF imaging has been shown to be a valuable tool to analyze disease progression and it may be beneficial to monitor therapeutic interventions [18]. Correlating findings on SD-OCT with

those on FAF imaging is likely to advance the understanding of underlying disease processes leading to an abnormal FAF signal. Besides FAF, other imaging modalities such as confocal blue and infrared reflectance imaging have recently been shown to reveal specific changes in different disease entities or fundus changes [19, 20]. Combined imaging with an SD-OCT will allow one to further investigate the corresponding changes on a quasi-histological level.

Summary for the Clinician

- Simultaneous recordings of SD-OCT and various cSLO-imaging modes provide a better understanding of retinal diseases. The precise correlation of topographic (cSLO) and tomographic (OCT) images, and especially the re-placement of the OCT scans at exactly the same retinal location in follow-up exams, allow a more reliable clinical evaluation of the disease evolution and treatment effects compared with the previous technologies.

References

1. Podoleanu AG, Rosen RB (2008) Combinations of techniques in imaging the retina with high resolution. Prog Retin Eye Res 27:464–499
2. Schmitz-Valckenberg S, Holz FG, Bird AC, Spaide RF (2008) Fundus autofluorescence imaging: review and perspectives. Retina 28:385–409
3. Helb HM, Charbel Issa P, Fleckenstein M et al (2009) Clinical evaluation of simultaneous confocal scanning laser ophthalmoscopy imaging combined with high-resolution spectral-domain optical coherence tomography. ActaOphthalmologica[inpress];DOI:10.1111/j.1755-3768.2009.01602.x
4. Jorzik JJ, Bindewald A, Dithmar S, Holz FG (2005) Digital simultaneous fluorescein and indocyanine green angiography, autofluorescence, and red-free imaging with a solid-state laser-based confocal scanning laser ophthalmoscope. Retina 25:405–416
5. Brar M, Bartsch DU, Nigam N et al (2009) Colour versus grey-scale display of images on high-resolution spectral OCT. Br J Ophthalmol 93:597–602
6. Charbel Issa P, Finger RP, Holz FG, Scholl HPN (2009) Multimodal imaging including spectral domain OCT and confocal near infrared reflectance for characterisation of outer retinal pathology in pseudoxanthoma elasticum. Invest Ophthalmol Vis Sci [in press]; DOI: 10.1167/iovs.09-3541
7. Li D, Kishi S (2009) Restored photoreceptor outer segment damage in multiple evanescent white dot syndrome. Ophthalmology 116:762–770
8. Spaide RF, Koizumi H, Freund KB (2008) Photoreceptor outer segment abnormalities as a cause of blind spot enlargement in acute zonal occult outer retinopathy-complex diseases. Am J Ophthalmol 146:111–120
9. Feng W, Yasumura D, Matthes MT, LaVail MM, Vollrath D (2002) Mertk triggers uptake of photoreceptor outer segments during phagocytosis by cultured retinal pigment epithelial cells. J Biol Chem 277:17016–17022
10. Dowling JE, Sidman RL (1962) Inherited retinal dystrophy in the rat. J Cell Biol 14:73–109
11. Charbel Issa P, Bolz HJ, Ebermann I, Domeier E, Holz FG, Scholl HP (2009) Characterization of severe rod-cone dystrophy in a consanguineous family with a splice site mutation in the MERTK gene. Br J Ophthalmol 93: 920–925
12. Fleckenstein M, Charbel Issa P, Helb HM et al (2008) High resolution spectral domain-OCT imaging in geographic atrophy associated with age-related macular degeneration. Invest Ophthalmol Vis Sci 49:4137–4144
13. Wolf-Schnurrbusch UE, Enzmann V, Brinkmann CK, Wolf S (2008) Morphologic changes in patients with geographic atrophy assessed with a novel spectral OCT-SLO combination. Invest Ophthalmol Vis Sci 49: 3095–3099
14. Barthelmes D, Sutter FK, Gillies MC (2008) Differential optical densities of intraretinal spaces. Invest Ophthalmol Vis Sci 49:3529–3534
15. Charbel Issa P, Foerl M, Helb HM, Scholl HP, Holz FG (2008) Multimodal fundus imaging in foveal hypoplasia: combined scanning laser ophthalmoscope imaging and spectral-domain optical coherence tomography. Arch Ophthalmol 126:1463–1465
16. Delori FC, Dorey CK, Staurenghi G, Arend O, Goger DG, Weiter JJ (1995) In vivo fluorescence of the ocular fundus exhibits retinal pigment epithelium lipofuscin characteristics. Invest Ophthalmol Vis Sci 36:718–729
17. Holz FG, Bellmann C, Staudt S, Schütt F, Völcker HE (2001) Fundus autofluorescence and development of geographic atrophy in age-related macular degeneration. Invest Ophthalmol Vis Sci 42:1051–1056
18. Holz FG, Bindewald-Wittich A, Fleckenstein M, Dreyhaupt J, Scholl HP, Schmitz-Valckenberg S (2007) Progression of geographic atrophy and impact of fundus autofluorescence patterns in age-related macular degeneration. Am J Ophthalmol 143:463–472
19. Charbel Issa P, Berendschot TT, Staurenghi G, Holz FG, Scholl HP (2008) Confocal blue reflectance imaging in type 2 idiopathic macular telangiectasia. Invest Ophthalmol Vis Sci 49:1172–1177
20. Weinberger AW, Lappas A, Kirschkamp T et al (2006) Fundus near infrared fluorescence correlates with fundus near infrared reflectance. Invest Ophthalmol Vis Sci 47: 3098–3108